Microscopic Study of a Ligand Induced Electroless Plating Process onto Polymers

Alexandre Garcia,*,†,‡ Thomas Berthelot,† Pascal Viel,‡ Jérôme Polesel-Maris,§ and Serge Palacin‡

LSI Irradiated Polymers Group (UMR 7642 CEA/CNRS/Ecole Polytechnique), CEA, IRAMIS, F-91128 Palaiseau Cedex, France, and SPCSI Chemistry of Surfaces and Interfaces Group and SPCSI Oxides Interfaces and Surfaces Group, CEA, IRAMIS, F-91191 Gif-sur-Yvette, France

ABSTRACT The ligand induced electroless plating (LIEP) process was recently developed and thoroughly demonstrated with one of the most used polymers for plating processes: acrylonitrile-butadiene-styrene (ABS). This generic process is based, thanks to the use of diazonium salts as precursors, on the covalent grafting of a thin layer of poly(acrylic acid) (PAA) acting as ligand for metallic salts onto pristine polymer surfaces. This strategy takes advantage of the PAA ion exchange properties. Indeed, carboxylate groups contained in PAA allow one to complex copper ions which are eventually reduced and used as catalysts of the metallic deposition. Essentially based on ABS, ABS-PC (ABS-polycarbonate) and PA (polyamide) substrates, the present paper focuses on the role of the polymer substrate and the relationships between the macroscopic properties and microscopic characterizations such as infrared (IR), X-ray photoelectron spectroscopy (XPS), atomic force microscopy (AFM), and scanning electron microscopy (SEM). The adhesion strength of the metallic layer deposited via that LIEP process with the bulk polymer substrates was successfully compared with the adhesion of similar copper films deposited by the usual process based on chromic acid etching and palladium-based seed layer, by measuring the T-peel adhesion strength, and by carrying out the common industrial scotch tape test. Lastly, the electrical properties of the deposited layer were studied thanks to a four-point probe and scanning tunneling microscopy (STM) measurements.

KEYWORDS: polymer electroless plating • metallization • electrical properties • adhesion • ABS • ABS-PC • polyamide and diazonium salts

1. INTRODUCTION

As materials interact with their environment via their surface, coating a metallic layer onto a polymer is a clever way to keep many properties brought by metals (conductivity, reflectivity, robustness versus mechanical stress) while reducing both the weight of the final objects and the costs associated with their manufacturing (transformation steps, polishing, transport). Electroless metal plating is the most used method to metallize insulating surfaces and more specifically polymers for the deposition of conformal metal films onto all-shaped substrates (1−5). Hence, nickel and electroless plating of polymers is of major importance in many fields including automotive, aerospace, microelectronics, decoration, and luxury packaging industries.

Common electroless processes involve three main steps: (i) surface preparation, (ii) surface activation or surface seeding with a catalyst, and (iii) the electroless deposition itself, which is the chemical deposition of a metal film from a solution containing a mild reducing agent and an ionic complex of the metal to be plated onto the seeded substrate (1, 2). Almost all the metals of the Group IB and VIII of the periodic table (Au, Pt, Ni, Cu, Co, Fe, etc.) can be plated and exhibit autocatalytic behavior. Hence, the electroless metal deposition is not stopped once the catalyst is covered by the first metal deposit (1, 2). Electroless deposition is actually a complex process involving multiple and simultaneous redox processes on the substrate surface in which composition, structure, and morphology are increasingly changing because of the plating. Besides, mechanistic details of metal deposition remain still unclear. The mixed potential theory (6) is perhaps the most used and experiment-based model for electroless metal deposition and consists of an initial spontaneous oxidation of the reducing agent at a catalytic surface, leading to electron charging of the substrate surface until its electrochemical potential becomes sufficiently negative to reduce the metallic complex to metal. The mixed potential theory provides a correct description of the electroless plating mechanism when electron transfer between the reducing agent and the metallic ion is mediated by the activated surface and can be described by diffusion controlled or electrochemically controlled partial reaction currents (6, 7). However, the mixed potential theory is not valid when an electron transfer can directly occur between the reducing agent and the metallic ion contained in the electroless plating bath, which is usually prevented by the use of a stabilizer. The latter prevents spontaneous reduction in solution (1). More recently, improved electroless deposition models on the different mechanistic steps were issued (8−11).

* Corresponding author. E-mail: alexandre.garcia@cea.fr. Phone: 00 33 1 69 08 12 80.
Received for review June 9, 2010 and accepted October 13, 2010
† LSI Irradiated Polymers Group (UMR 7642 CEA/CNRS/Ecole Polytechnique), CEA, IRAMIS.
‡ SPCSI Chemistry of Surfaces and Interfaces Group, CEA, IRAMIS.
§ SPCSI Oxides Interfaces and Surfaces Group, CEA, IRAMIS.
DOI: 10.1021/am100907j
2010 American Chemical Society

ARTICLE

In the electroless plating industry, noble metal Pd is commonly employed as catalyst to initiate the electroless deposition previously described (7, 12−14). Taking into account that the cost of palladium has been raised in recent years, the development of Pd-free catalysts has attracted a lot of attention lately (15−19), and copper has been proposed as an alternative catalyst (20−22).

For acrylonitrile-butadiene-styrene (ABS), ABS-PC (polycarbonate) and PA (polyamide) which represent more than 90% of the polymers industrially metallized, metal plating with an adherent metallic layer is only possible if an appropriate etchant system is previously employed for surface conditioning (23−33). The surface preparation step, thus, aims at (i) increasing the bulk polymer wettability by surface oxidation and (ii) increasing the bulk polymer roughness in order to improve the surface seeding of the electroless catalyst and the adhesion of the final metallic layer. Up to now, the best (and most widely used) method is based on a chromic acid etching, which oxidizes the bulk polymer surface (2, 23, 25, 26). These oxidation phenomena imply both chemical and mechanical adhesion, respectively, thanks to the chemical reactive group formation and the superficial hole or cavity creation which increases the surface roughness. However, because of the future European ban on chromium waste, that efficient process has to be replaced (34, 35). Recent works, based on a technological breakthrough, consist of the formation of a robust interphase between the substrate surface and the metallic layer which is intended to replace the rough interface which usually results from the chromic acid treatment (22, 36−39). For example, block copolymers with one block designed to interpenetrate the polymer substrate and the other one bearing chelating groups (such as poly(acrylic acid) (PAA)) were recently used to form a host polymer film for electroless plating on various polymer substrates (40). That innovative method, however, requires the synthesis of a two-block copolymer in which one block is made of the same polymer as the substrate (or highly miscible with it), and another one bears chelating groups for the catalyst precursor. As shown in Figure 1, the ligand induced electroless plating (LIEP) process is, on the contrary, based on the covalent grafting of a thin chelating polymer film from its monomer precursors onto a polymer substrate. In that case, the process does not require the synthesis of a designated reactant, and the resulting polymer film is covalently grafted to the substrate and able to complex copper ions which are then reduced and act as catalyst for the growth of the metallic phase which starts inside the host polymer. On these grounds, we recently reported the electroless plating of copper and nickel on ABS polymers based on the one-step covalent grafting of a poly(acrylic acid) (PAA) thin polymer film by the GraftFast process (22, 31, 41). Beyond the adhesive benefits describe above, the LIEP process can be applied to a wide range of polymers since the GraftFast process is a powerful toolset to graft covalent polymer films onto various substrates based on the chemical reduction of aryldiazonium salts (22, 31, 41).

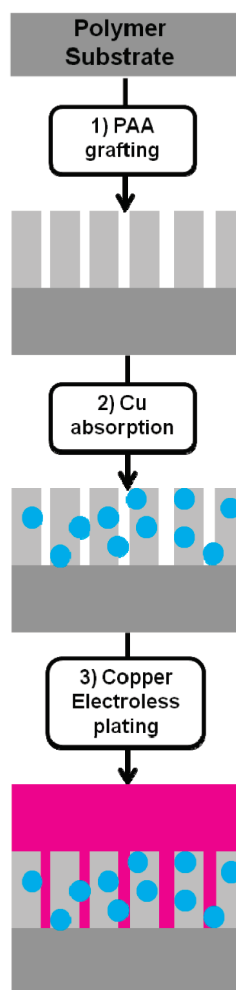

FIGURE 1. Schematic view of the LIEP process: (1) surface modification via the PAA grafting, (2) surface activation through the copper absorption (Cu chelation + reduction), and (3) growth of the Cu plated film thanks to the use of the electroless copper plating bath.

The present paper focuses on the influence of the chemical nature of the polymer substrate on the final metallic layer. We first studied the LIEP process onto the three individual components of the ABS copolymer (i.e., polyacrylontrile (PAN), polybutadiene (PB), and polystyrene (PS)). Then, we demonstrate that the LIEP process applies successfully to ABS-PC and PA, two polymers which are structurally very different. On both polymers, PAA grafting was demonstrated together with its effect on the metallic layer adhesion strength. Cu^{2+} ion complexation and reduction and copper electroless deposition steps were fully characterized. The electrical properties of the plated copper layer were studied by scanning tunneling microscopy (STM) measurements, and the plated copper resistivity was measured by a four-point probe. On the basis of these characterizations and the one carried out onto ABS substrates in our previous paper, we were able to decipher the role of the substrate chemical structure and its surface morphology on the PAA grafting and the plated copper layer.

2. EXPERIMENTAL SECTION

Materials. ABS, ABS-PC, and PA of technical quality were obtained from Pegastech S.A. as common test samples used in

the industrial field. An industrial detergent was used to clean the substrates: TFD4 (Franklab). 1-4-Diaminophenylene dihydrochloride (Fluka, ≥99%), acrylic acid (Sigma Aldrich, ≥99%), sodium nitrite (Fluka, ≥99%), and iron powder (Prolabo VWR, 98%) were used for the poly(acrylic acid) grafting using the GraftFast technology. Cupric sulfate $CuSO_4$, $5H_2O$ (Fluka, ≥ 99%), and sodium borohydride powder (Sigma Aldrich, ≥98.5%) were used for the catalytic copper chelation and reduction. Then, for the electroless metal deposition, an industrial copper plating bath (M Copper 85 supplied by MacDermid) was used.

Electroless Metal Deposition Process. As shown in Figure 1, the LIEP process is divided into three steps as discussed in the following three sections.

Covalent Grafting of Poly(acrylic Acid) on Polymer Substrates. All the polymer substrates were sonicated for 30 min into an industrial detergent (TFD4) and thoroughly rinsed in deionized water. Then, 1-4-phenylenediammonium dihydrochloride was dissolved in a 0.5 M HCl solution to obtain 100 mL at 0.1 M (Solution 1). Under stirring, 21 mL of $NaNO_2$ (0.1 M) was added stepwise to 35 mL of Solution 1 in order to synthesize the aryldiazonium salt. At this stage, the $NaNO_2$/1-4-phenylenediammonium molar ratio was equal to 0.6. Acrylic acid (10 mL) was then introduced into this solution. Polymer substrates (4 × 1 × 0.2 cm) were introduced in the beaker, and iron powder (5.25 g) was added to the solution. After 5, 10, 20, 30, and 40 min, 2 mL of $NaNO_2$ (0.1M) was added to the solution. At the end, the $NaNO_2$/1-4-phenylenediammonium dihydrochloride molar ratio reached ca. 0.9. That stepwise addition promoted a continuous aryldiazonium salt formation and subsequently a continuous phenyl radical formation; hence, both polyphenylene and poly(acrylic acid) polymerizations could be initiated all along the reaction. After immersion for 90 min at 38 °C, polymer substrates were sonicated twice for 10 min in alkaline solution (NaOH, 1 M) and deionized water. The rinsing treatment allowed one to discard most of the physisorbed matter, as evidenced by the subsequent stability of the infrared (IR) absorption bands of PAA upon further rinsing.

Chelation and Reduction of Metallic Cations. PAA-modified polymer substrates were immersed for 5 min into an alkaline (NH_3, 0.6 M) copper sulfate $CuSO_4 \cdot 5H_2O$ (0.1 M) solution at room temperature to induce an ion-exchange process. Afterward, samples were rinsed with deionized water. In order to reduce Cu^{2+} ions previously chelated by the carboxylate groups contained in grafted PAA films, modified substrates were immersed into a sodium borohydride ($NaBH_4$) (0.1M)−NaOH (0.1 M) solution at 40 °C for 10 min.

Electroless Copper Deposition. The surface-activated substrates were finally placed in the industrial copper electroless metal plating bath (M Copper 85). That commercial plating bath required the addition of a reducing agent just before the plating step. Formaldehyde HCHO was used as the reducing agent; optimum conditions were obtained with a copper content of 2 $g \cdot L^{-1}$, a mass ratio HCHO/Cu of 2, a pH at 13, a work temperature at 48 °C. The observed deposition rate was about 4 μm/h. Polymer substrates were left in the bath for 15 min.

3. CHARACTERIZATIONS

Characterization Methods. Infrared spectra were recorded on a Bruker Vertex 70 spectrometer equipped with an attenuated total reflection (ATR) Pike-Miracle accessory. The MCT detector:Hg-Cd-Te (MCT) detector working at liquid nitrogen temperature. The spectra were obtained after 256 scans at 2 cm^{-1} resolution.

X-ray photoelectron spectroscopy (XPS) studies were performed with a KRATOS Axis Ultra DLD spectrometer, using the monochromatized Al Kα line at 1486.6 eV. The pass energy of the analyzer was kept constant at 20 eV for C_{1s} core level scans. The photoelectron takeoff angle was 90° with respect to the sample plane, which provides an integrated sampling probe depth range going from 7 to 20 nm for our substrates.

Atomic absorption spectroscopy was carried out on a Thermo Fisher Scientific Atomic Absorption Spectrometer (ICE 3000 Series) with a hollow cathode lamp for Co−Cu−Mn−Ni at a primary wavelength of 324.8 nm and a bandpass of 0.5 nm using an air−acetylene flame at a gas flow rate of 0.9 L/min and a 10 wt % HNO_3/deionized water matrix. The lamp current was 7.5 mA.

Pristine polymer substrates were imaged by atomic force microscopy (AFM) in acoustic mode with a Molecular Imaging PicoSPMLe commercial AFM microscope (PicoScan 2100 controller, Scientec, France) using a commercial pyramidal Si tip (mounted on a 225 μm long single-beam cantilever with a resonance frequency of approximately 75 kHz and a spring constant of about 3 $N \cdot m^{-1}$). The scan rate was in the range of 0.25 Hz with a scanning density of 512 lines per frame. The AFM was mounted on a floating table to achieve vibration insulation during investigations. The root mean square (rms) roughness values of the scans were calculated using the Gwyddion 2.19 program covered by GNU General Public License.

Tunneling current spectroscopy characterization and high resolution AFM imaging of copper plated surfaces have been performed on a VT-AFM (Omicron GmbH) working in an ultra high vacuum environment at room temperature. This microscope has been modified to work with piezoelectric QPlus sensors (47) with etched Pt/It tip in order to combine AFM and STM imaging on the same conductive sample. To ensure the surface conductivity through the substrate, conductive silver ink was deposited between the studied surface and the conductive STM platform.

A four-point probe (S302K-LRM, Lucas Lab) was used to measure the resistivity of the plated metallic layers. The scanning electron microscopy images were recorded by a Hitachi S4800 equipped with a Field Emission Gun (FEG-scanning electron microscopy (SEM)) and coupled with an energy dispersive X-ray spectrometer (EDX).

Mechanical Adhesion Test. The adhesion between the plated metallic layer and the ABS-PC and PA substrates was studied by two different mechanical adhesion tests. The first method was a T-peel strength adhesion measurement, based on the standard test method for peel resistance of adhesives (T-peel test) ASTM D1876-08, measured thanks to the MTS Fundamental 90° Peel Fixtures Synergie 100 device. The second method was the standard ASTM D3359 Scotch tape test (cross-cut tape test) which consists of applying and removing pressure-sensitive adhesive tape over 16 cross-hatched squares of 1 × 1 mm^2 made in the film thanks to an Elcometer Cross Hatch cutter (Elcometer 107 X-Hatch ASTM Kit). That standard well-used test allows a direct comparison of the adhesion of films obtained under various conditions on similar substrates.

Table 1. O/C Ratio before and after PAA Grafting and Roughness on Pristine Polymers

	O/C ratio on pristine polymers	O/C ratio after PAA grafting + Cu^0	roughness$_{rms}$ (nm) for a 2 × 2 μm^2 area
ABS	0.03	0.17	38 ± 6
ABS-PC	0.28	0.34	28 ± 6
PA	0.14	0.35	112 ± 8
pure PAA	0.4		

4. RESULTS AND DISCUSSION

PAA Covalent Grafting and Cu^{2+} Chelation and Reduction. Like in the ABS case (22), poly(acrylic acid) has been covalently grafted onto all the substrates via the GraftFast process (31, 41) which relies on the redox activation of in situ synthesized aryldiazonium salts. Aryl radicals issued from the chemical reduction of aryldiazonium salts act both as initiators for the radical polymerization of acrylic acid and as direct source of a polyphenylene primer sublayer. In a previous paper (41), it has been proposed that, once the polyphenylene adhesion primer layer is covalently grafted to the polymer substrates, the interaction of growing oligoradical chains with the polyphenylene-like primer layer gives a grafted copolymer film. The growth of the poly(acrylic acid) film is then induced by the successive grafting of oligoradical chains and phenyl groups embedded in the already grafted chains. In order to initiate the poly(acrylic acid) radical polymerization, aryl radicals were produced all along the reaction by the successive additions of $NaNO_2$. $NaNO_2$ induces the aryldiazonium salt formation which is then reduced in aryl radical by the iron powder contained in solution. This PAA grafting was clearly observed by IR and XPS spectroscopy, and the same conclusions as in the case of the ABS substrates could be done (22). For details, see the Supporting Information.

The role of the polymer substrates on the PAA grafting was first evaluated by comparing the PAA grafted films obtained on PAN, PB, and PS, which are the three individual components of ABS (see Supporting Information). Thanks to contact angle measurements and IR and XPS analyses, PAA grafting was obviously promoted onto PAN substrate which is also more hydrophilic than PB and PS (42, 43). Those results give a first indication on the influence of the substrate properties (in particular its hydrophilic behavior) on the PAA grafting.

Then, PAA grafting was evaluated on ABS, ABS-PC, and PA. First, the PAA grafting efficiency was estimated thanks to the O/C ratio measured from the XPS spectra. Indeed, an increase of that ratio is expected upon the PAA grafting, since the O/C ratio is 0.4 for pure PAA, and only 0.03, 0.28, and 0.14 for pristine ABS, APS-PC, and PA, respectively. As indicated by Table 1, XPS spectra of the PAA-grafted polymers exhibit a significantly higher increase for the O/C ratio in the case of PA than for ABS and ABS-PC.

This result confirms the study of the PAA grafting onto PAN, PB, and PS: the PAA grafting appears promoted on hydrophilic substrates. This behavior is likely to arise from the better swelling of the surface of a hydrophilic substrate, with respect to a hydrophobic one such as PS or PB, by the

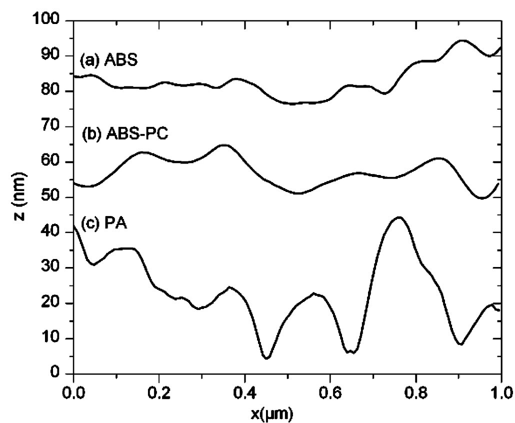

FIGURE 2. One micrometer profile extraction of pristine ABS (a), ABS-PC (b), and PA (c) substrates.

aqueous reactive mixture which is used for the PAA grafting step. In the case of the ABS and ABS-PC which are both composite materials containing both hydrophilic (PAN, PC) and hydrophobic (PB, PS) polymers, we can assume local disparities in the PAA grafting efficiency, depending on the surface composition, since the PAA grafting is more efficient on PAN and polycarbonate which are more hydrophilic than on PS and PB.

However, this higher O/C ratio for PA may also be attributed to the influence of surface roughness, measured thanks to AFM analysis, which is around three times higher for the PA substrate than for the ABS and ABS-PC ones at the micrometer scale, as shown in Table 1 and Figure 2. A higher roughness obviously induces the increase of the actual contact area with the reactive solution. Thereby, more PAA oligoradicals can be grafted onto the substrate surface for a given projected area probed by XPS or IR analysis.

Hence, we assume that both the morphology and the chemical composition of the surface of the pristine substrate play a key role in the density and homogeneity of the final grafted-PAA film.

This higher PAA grafting rate for PA substrates than for ABS and ABS-PC has a direct influence on the amount of loaded copper ions after immersion into an alkaline solution containing ammonia and $CuSO_4$. The copper ions surface concentration Γ ($\mu g \cdot cm^{-2}$) was measured by flame atomic absorption spectroscopy on 80 cm^2 substrates. After an immersion time of 5 min in the alkaline solution, the Cu^{2+} loaded substrates were immersed during 10 min into a 10 wt % HNO_3/deionized water solution. As expected from the pH-switchable chelating properties of PAA, the copper ions were totally released from the polymer film in the acidic bath. Flame atomic absorption spectroscopy on the acidic bath containing the copper species released from the films allows an accurate measurement of the pristine surface concentration of copper species within the grafted films at equivalent roughness. As shown in Table 2, for ABS and ABS-PC substrates, the final copper ions surface concentration Γ was measured at ca. 1 $\mu g \cdot cm^{-2}$ whereas for PA substrates, the amount of loaded Cu^{2+} was more than 10 times higher. Besides, the PA substrates blue color, visible with the naked eye, was a clear indication of the high amount of loaded

Table 2. Cu^{2+} Surface Coverage after Chelation and Cu Atomic Percentage after Chelation and Reduction

	Γ after chelation at equivalent roughness ($\mu g \cdot cm^{-2}$)	% Cu after chelation	% Cu after reduction
ABS	0.9 ± 0.2	2	2
ABS-PC	0.6 ± 0.2	1	0.8
PA	14.6 ± 2.8	7	4

Cu^{2+}. To a lesser extent, this high difference in the amount of loaded Cu^{2+} was also observed by Cu_{2p} XPS analysis since the Cu atomic percentage derived from the XPS spectra was 7 % for PA substrates and only 2 % and 1 % for ABS and ABS-PC, respectively. Nevertheless, it is difficult to directly compare both evaluations (XPS and flame atomic absorption) in that case. Indeed, for flame atomic absorption which measures the copper species spontaneously adsorbed and then chemically released from the PAA grafted film, the analysis is unaffected by the surface morphology and the PAA actual thickness, whereas for XPS quantitative analysis, the average sampling probe depth is affected by the PAA layer morphology and the roughness. In other words, for the thicker PAA grafted films, a difference may be observed between XPS and flame absorption, because the sampling volume is not the same. Moreover, the analysis area differences (80 cm^2 for flame atomic absorption and less than 1 mm^2 for XPS analysis) can also be responsible for some differences in the copper evaluation, despite our XPS measurements were always averaged from two different analyses.

That higher copper loading also showed up after the reduction step. As shown in Figure 3, for both ABS-PC and PA substrates, after immersion into a $NaBH_4$ solution, the peaks of $Cu_{2p3/2}$ and $Cu_{2p1/2}$ core level binding energies confirmed the copper reduction (44). The catalytic-Cu^0 atomic ratio was measured at 2 % for ABS, 0.8 % for ABS-PC, and 4 % for PA. It is noteworthy that the difference observed between PA and the two other substrates is lower after than before reduction. A significant part of the copper species absorbed within the PA/PAA substrates seems to be released in solution upon the reduction step. That may arise from the higher roughness of PA substrates (when compared to ABS and ABS-PC): Indeed, we assume that copper species (likely copper sulfate $CuSO_4$) are actually adsorbed but unchelated at the outer surface of the grafted PAA films. That phenomenon is obviously promoted by the high roughness for the PA/PAA surfaces, since adsorption is easier on complex geometries. A low amount of sulfur was indeed observed on the XPS spectra recorded after the chelation step on PA/PAA samples (data not shown), which clearly indicates that some unchelated copper species are present. Those "extra" copper species (with respect to the copper ions actually chelated by carboxylate anions within the PAA chains) explain the large difference between the copper loading after the chelation step between PA (high roughness) and ABS or ABS-PC (low roughness). After the reduction step, all copper species are reduced to Cu^0, since we did not observe any Cu^{II} signal in the XPS spectra. The Cu^0 species derived from previously chelated copper ions are physically trapped within the PAA chains, while the Cu^0 species arising from the copper salts only adsorbed on the outer parts of the films are only weakly linked and are likely to be more easily discarded by the rinsing steps. Hence, the high difference in copper loading observed after the chelation step between PA and ABS or ABS-PC decreases after the reduction step, as shown by Table 2.

Assuming that all chelated copper ions were retained in the polymer film during the reduction step, it was possible to estimate the carboxylate groups chelation rate by copper ions contained in the PAA films. On the basis of the Cu_{2p}/COOH C_{1s} atomic ratio evaluated by XPS analysis after reduction and given that one copper ion should normally be chelated by two carboxylate groups COO^-, between 70 % and 80 % of the carboxylate groups were occupied by copper ions whatever the substrate, which means that the PAA ion exchange properties are very efficient for copper seeding and the differences observed and previously described on the copper loading are thus directly linked to the higher PAA grafting on PA substrates.

Electroless Copper Deposition. Taking into account all the parameters described in the Experimental Section,

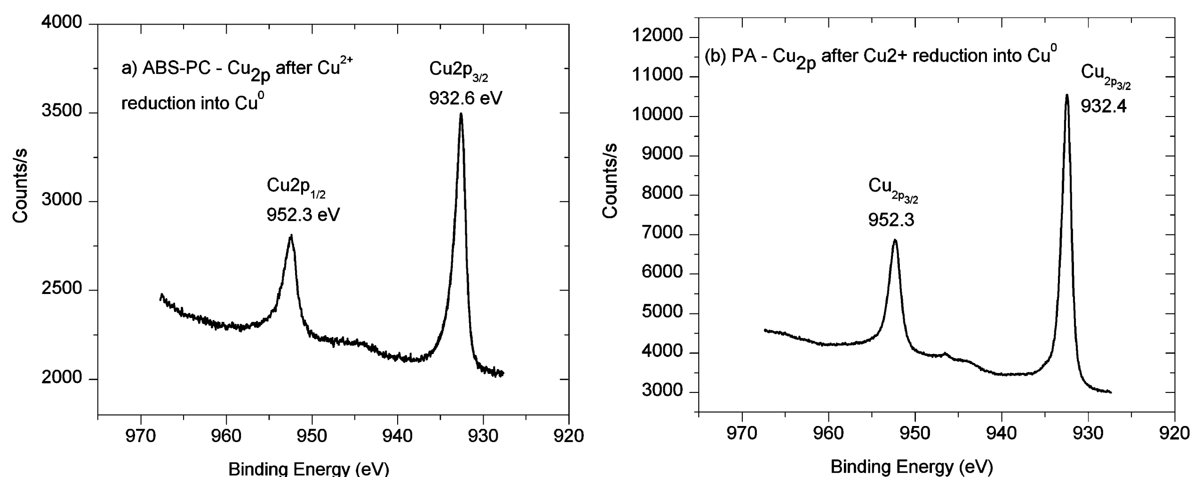

FIGURE 3. Cu_{2p} XPS spectra of ABS-PC (a) and PA (b) substrates after the reduction step.

immersing the Cu-activated substrates in the M Copper 85 industrial copper plating bath during 15 min allowed the formation of 1 μm-thick plated-copper films. It might be surprising that the plated-copper thickness was the same whatever the pristine substrates, since we demonstrated in the previous sections that more copper catalyst was formed on PA than on ABS or ABS-PC. Actually, as the electroless plating process is autocatalytic, the growth speed becomes constant once the first nanometers of plated copper are formed. The amount of catalytic copper does not seem to have any influence there (1, 45).

The obtained plated layers were characterized by XPS measurements. Again, as in the ABS case (22), Cu_{2p} spectra indicate that a plated Cu^0 layer was successfully formed on the ABS-PC and PA substrates (for details, see the Supporting Information). As expected, the Cu atomic percentage after the electroless plating was widely superior to the one obtained after reduction and around 30%. In both cases, oxygen and carbon elements were still present, due to organic residuals coming from the plating bath and in particular from the complexing agent, but they cannot be attributed to the underlying polymers because the plated copper layers were too thick to allow XPS to probe underlying species.

SEM images in Figure 4 showed that, for both ABS-PC and PA substrates, the metallic layer consists of a tight, dense, continuous, and void-free structure which is required for the following electroplated steps. Like in the ABS-PC case, the Cu-plated PA section showed a global homogeneous metallic top layer and a good interfacial zone between the plated metal and the substrate. Finally, whatever the substrate, the final metallic layer thickness was evaluated around 1 μm after a 15 min plating step.

EDX spectra analysis for Cu-plated PA substrates also revealed that the metallic layer surface is composed only of Cu^0 (for details, see the Supporting Information). Besides, the electrical resistivity of the as-plated copper measured by the four-point probe method was evaluated to be slightly higher than bulk copper (1.67 $\mu\Omega \cdot$ cm) (46): 3.2 $\mu\Omega \cdot$ cm for ABS, 2.54 $\mu\Omega \cdot$ cm for ABS-PC, and 2.15 $\mu\Omega \cdot$ cm for PA. The presence of defects and hydrogen entrapment in the films are the major factors contributing to the observed increase in the resistivity of the plated films, with respect to bulk pure copper (47). According to the obtained results, PA is the substrate which gave the best results from an electrical point of view. However, for both cases, STM and AFM images are really similar. Indeed, even if, in the PA case, the copper layer is more conductive, these STM images showed that on both PA and ABS-PC substrates the plated copper layers are conductive all over the substrate which is important for many applications. I−V tunneling current spectroscopy curves showed also a metallic behavior on both cases (for details, see Supporting Information).

As observed on the SEM images, AFM analysis showed that the plated copper particle size is almost three times lower in the case of PA substrate (ca. 40 nm) than in the ABS-PC case (Figure 5) (48). The grain size of the electroless plated layers is dependent on the catalyst one (1, 49). Indeed, the lower and more homogeneous the catalyst particles, the lower is the grain size of the electroless plated layer. In the PA case, the grain size of the electroless copper plated layers is three times lower than in the ABS-PC one, which suggests that the catalytic-Cu^0 particles size is lower

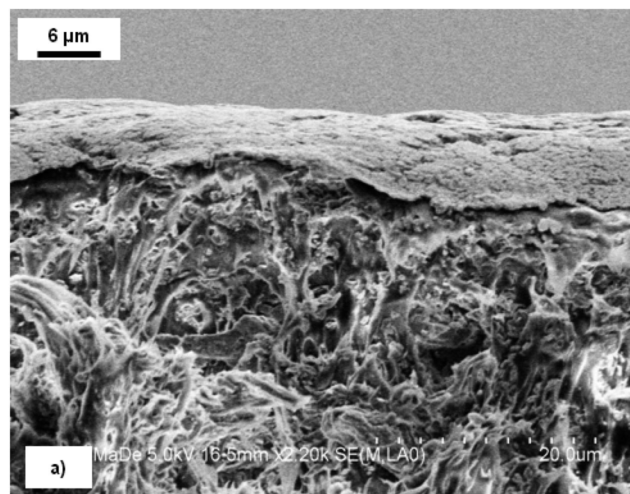

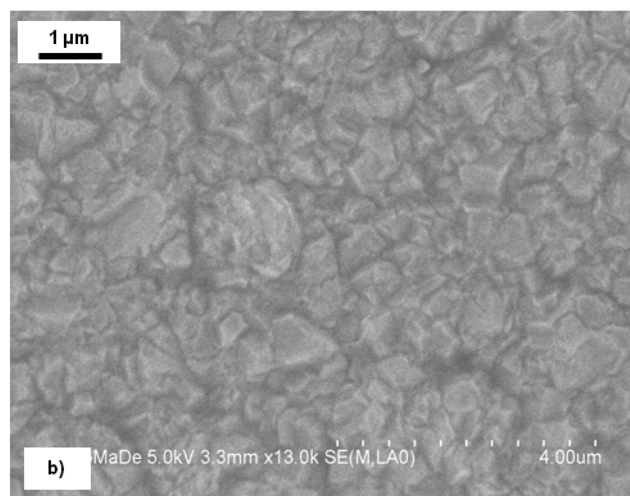

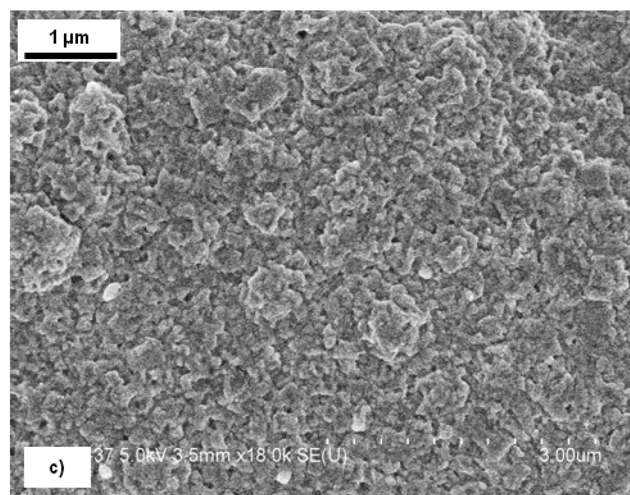

FIGURE 4. SEM images after electroless copper plating: PA section (a) and ABS-PC (b) and PA (c) top views. The scales are given on the images.

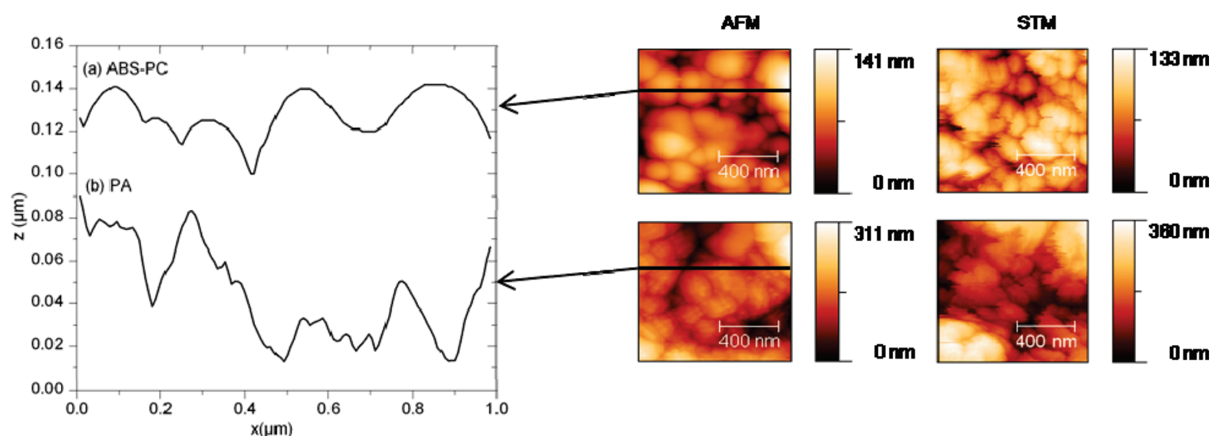

FIGURE 5. One × one micrometer AFM and STM images of Cu-plated ABS-PC (top) and PA (bottom) substrates with the corresponding profile extractions on the left.

and more homogeneous. This is supported by the fact that, in the PA case, the PAA layer is more homogeneous all over the substrate and more compact which allows one to obtain lower-size Cu-catalyst particles. The hydrophilic and rough surface of PA substrates promote the PAA grafting, and the obtained compact PAA chains involves the formation of lower and more homogeneous Cu-catalytic particles and lower Cu-plated grain size than for ABS-PC and ABS substrates. In the ABS-PC and ABS cases, according to all the characterizations, the grafted-PAA layer seems to be less compact and heterogeneous; there are less Cu-catalytic particles, and they are not homogeneous which lead to higher Cu-plated grain size.

Lastly, as expected, the 1 μm-thick plated metallic film is quite conformal to the pristine surface, whatever the pristine polymer. Hence, at the same scale than for the pristine substrates (2 μm^2), the roughness after plating was equal to 38 nm for ABS-PC and 109 nm for PA. According to the roughness of the pristine substrates previously described (Table 1), the PA/PAA/Cu roughness is still around three times higher than in the ABS-PC case.

Finally, the adhesion between the metallic layer and the polymer substrates was studied by two different methods. First, T-peel strength adhesion measurements were carried out and the results were excellent since in both cases; the metallic layer was not removed. No quantitative conclusion can be derived from those results, except that the adhesion strength of our plated-copper layers is largely enough for many applications, since the T-peel strength measurement is a classical corner stone of industrial qualification for metal plating processes.

Second, the adhesion strength has been studied by the most common industrial adhesion test which is also among the most demanding one: the standard ASTM D3359 Scotch tape test. When the classical chromic acid etching-based process was used on our ABS-PC and PA samples, none of the 16 cross-hatched squares was removed. For ABS-PC substrates plated following the LIEP process, we observed the removal of almost half of the squares, as it was observed for ABS substrates (see Supporting Information). On the contrary, Figure 6 shows, for PA samples, no squares were removed, as for the classical chromium-based process. It is noteworthy that, when ABS-PC and PA were Cu-plated without any PAA-grafting or after spin-coating PAA from a 0.5% w/w solution (50), the same scotch test showed all the squares fully removed. These adhesion results can be attributed to the nanometer-scale mechanical interlocking effect, which mimics the micrometer-scale interdigitation that occurs between the metallic layer and the rough interface which results from the chromic acid treatment. The adhesion which is estimated by the Scotch tape test arises from two factors: (i) the strength of the interface between the PAA coating and the polymer substrate; (ii) the so-called "interlocking effect" between the copper metal film and its substrate.

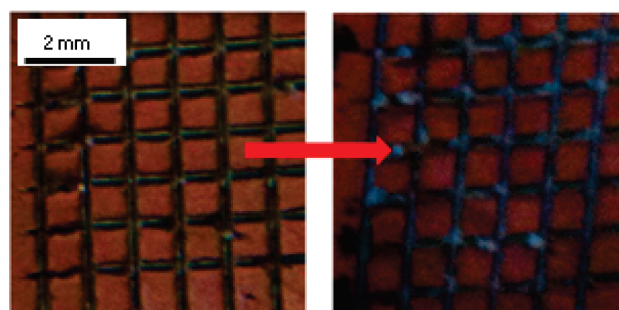

FIGURE 6. Images of a Cu-plated PA substrate before (left) and after (right) the scotch tape test.

As mentioned above, when PAA is spin-coated, most of the PAA layer is removed along with Cu after the scotch tape test. This is consistent with the absence of covalent bonding between the PAA coating and the substrate, taking into account the fact that, contrary to "classical electroless plating", the copper metal film grows within the PAA film and is thus only marginally in direct contact with the substrate. However, when comparing PAA films grafted on different polymers, that former factor should, at first sight, be considered as even. Actually, the roughness of the surface again plays a role here: As the scotch test consists of applying a constant force to peel out a given scotch tape test, the higher the roughness, the stronger is the actual strength of the polymer-to-PAA interface, because the actual number of covalent bonds between PAA and the substrate is higher on a rougher substrate for a given scotch area. That is a main

ARTICLE

reason to explain why PAA on PA exhibits no damages after the scotch tape test, when compared to ABS or ABS-PC substrates which are less rough.

Regarding now the interlocking effect, the actual thickness of the PAA coating obviously enhances its role in the observed adhesion. However, as the observed higher amount is likely to arise from the higher roughness of PA, we cannot conclude on the role of the interlocking effect in the differences observed between PA, PC, and ABS-PC in the scotch tape test.

When compared to the strength adhesion measured after the chromic acid etching-based process, our results appear quite promising for PA substrates but still insufficient for ABS and ABS-PC, at least for all the applications which require a strong adhesion of the plated layer. Nevertheless, further works are currently carried out to improve the adhesion strength, using only soft and ecological methods in order to keep consistent with our primary goal, i.e., replace the chromic acid surface activation step by a more ecological one. However, for other applications such as flexible electronics where the copper layers are directly recovered and protected after the electroless plating, the adhesion strength observed for ABS and ABS-PC should be sufficient.

5. CONCLUSIONS

In this paper, we thoroughly compared three industrially relevant plastics as substrates for our recently described LIEP process. We demonstrated that initial roughness and surface composition significantly influence the chemical grafting of a PAA film, which eventually complexes copper ions as precursors for electroless plating catalysis. We have been able to link the macroscopic properties of the final metal plated layer, such as the strength adhesion and the electrical resistivity to the microscopic properties of its precursor steps, such as the amount of loaded catalyst precursors and the morphology and the chemical composition of the surface of the pristine substrate. Indeed, our results show that the higher PAA grafting rate, the higher is the amount of loaded catalytic copper, the lower is the particle size in the plated copper film, and the higher is its conductivity. This work highly strengthens the versatility of the LIEP process, which relies on available monomers and reactants and applies directly to any polymer surface, and increases its application fields. Further works are currently being carried out to take advantage of the GraftFast step to localize the electroless metal plating and to apply it to other polymers.

Acknowledgment. The authors would like to thank Dr Vincent Mévellec (Alchimer) for his help in the resistivity and T-peel strength adhesion measurements.

Supporting Information Available: Complementary IR, XPS, and EDX spectroscopies, I_T-V_b spectroscopy curves, and ABS-PC scotch tape test images. This material is available free of charge via the Internet at http://pubs.acs.org.

REFERENCES AND NOTES

(1) Mallory, G. O.; Hajdu, J. B. *Electroless Plating: Fundamentals and Applications*; The American Electroplaters and Surface Finishers Society, Washington, DC, 1990.
(2) Sacher, E. *Metallization of Polymers 2*. Plenum Publisher: New York, 2002.
(3) Demirel, M. C.; Cetinkaya, M.; Singh, A.; Dressick, W. J. *Adv. Mater.* **2007**, *19*, 4495–4499.
(4) Ma, D. I.; Shirey, L.; McCarthy, D.; Thompson, A.; Qadri, S. B.; Dressick, W. J.; Chen, M. S.; Calvert, J. M.; Kapur, R.; Brandow, S. L. *Chem. Mater.* **2002**, *14*, 4586–4594.
(5) Price, R. R.; Dressick, W. J.; Singh, A. *J. Am. Chem. Soc.* **2003**, *125*, 11259–11263.
(6) Ohno, I. *Mater. Sci. Eng., A* **1991**, *146*, 33–49.
(7) Zouhou, A.; Vergnes, H.; Duverneuil, P. *Microelectron. Eng.* **2001**, *56*, 177–180.
(8) Chang, Y. L.; Ye, W. C.; Ma, C. L.; Wang, C. M. *J. Electrochem. Soc.* **2006**, *153*, C677–C682.
(9) Dimitrov, V.; Gorker, L. *Prog. React. Kinet. Mech.* **2006**, *31*, 45–58.
(10) Homma, T.; Tamaki, A.; Nakai, H.; Osaka, T. *J. Electroanal. Chem.* **2003**, *559*, 131–136.
(11) Shimada, T.; Nakai, H.; Homma, T. *J. Electrochem. Soc.* **2007**, *154*, D273–D276.
(12) Jiang, B. Q.; Xiao, L.; Hu, S. F.; Peng, J.; Zhang, H.; Wang, M. W. *Opt. Mater.* **2009**, *31*, 1532–1539.
(13) Nicolas-Debarnot, D.; Pascu, M.; Vasile, C.; Poncin-Epaillard, F. *Surf. Coat. Technol.* **2006**, *200*, 4257–4265.
(14) Charbonnier, M.; Romand, A.; Goepfert, Y.; Leonard, D.; Bessueille, F.; Bouadi, A. *Thin Solid Films* **2006**, *515*, 1623–1633.
(15) Charbonnier, M.; Romand, M.; Goepfert, Y. *Surf. Coat. Technol.* **2006**, *200*, 5028–5036.
(16) Dai, W.; Wang, W. J. *Sens. Actuators, A* **2007**, *135*, 300–307.
(17) Hsiao, Y. S.; Whang, W. T.; Wu, S. C.; Chuang, K. R. *Thin Solid Films* **2008**, *516*, 4258–4266.
(18) Matsumura, Y.; Enomoto, Y.; Sugiyama, M.; Akamatsu, K.; Nawafune, H. *J. Mater. Chem.* **2008**, *18*, 5078–5082.
(19) Miyoshi, K.; Aoki, Y.; Kunitake, T.; Fujikawa, S. *Langmuir* **2008**, *24*, 4205–4208.
(20) Bicak, N.; Karagoz, B. *Surf. Coat. Technol.* **2008**, *202*, 1581–1587.
(21) Charbonnier, M.; Romand, M.; Goepfert, Y.; Leonard, D.; Bouadi, M. *Surf. Coat. Technol.* **2006**, *200*, 5478–5486.
(22) Garcia, A.; Berthelot, T.; Viel, P.; Mesnage, A.; Jegou, P.; Nekelson, F.; Roussel, S.; Palacin, S. *ACS Appl. Mater. Interfaces* **2010**, *2*, 1177–1183.
(23) Mance, A. M. *J. Electrochem. Soc.* **1992**, *139*, 724–728.
(24) Brandes, M.; Fels, C. C. *Met. Finish.* **2008**, *106*, 21–24.
(25) Wang, G. X.; Li, N.; Hu, H. L.; Yu, Y. C. *Appl. Surf. Sci.* **2006**, *253*, 480–484.
(26) Wang, G. X.; Li, N.; Li, D. Y. *J. Univ. Sci. Technol. Beijing* **2007**, *14*, 286–289.
(27) Charbonnier, M.; Romand, M. *Int. J. Adhes. Adhes.* **2003**, *23*, 277–285.
(28) Esrom, H.; Seebock, R.; Charbonnier, M.; Romand, M. *Surf. Coat. Technol.* **2000**, *125*, 19–24.
(29) Kupfer, H.; Hecht, G.; Ostwald, R. *Surf. Coat. Technol.* **1999**, *112*, 379–383.
(30) Dillard, D.; Maquire, E.; Donovan, L. U.S. Patent 4,335,164, 1982.
(31) Mévellec, V.; Roussel, S.; Deniau, G. FR Patent 2,910,006, 2007.
(32) Jacob, G. U.S. Patent 3,733,213, 1973.
(33) Hiroshi, N. EU Patent 1,148,153, 2001.
(34) European Parliament and the Council, 2002/95/EC, Brussels, 2003.
(35) European Parliament and the Council, 2005/90/EC, Brussels, 2006.
(36) Aldakov, D.; Bonnassieux, Y.; Geffroy, B.; Palacin, S. *ACS Appl. Mater. Interfaces* **2009**, *1*, 584–589.
(37) Li, L.; Yan, G. P.; Wu, J. Y.; Yu, X. H.; Guo, Q. Z.; Kang, E. T. *Appl. Surf. Sci.* **2008**, *254*, 7331–7335.
(38) Liaw, W. C.; Huang, P. C.; Chen, K. P.; Chen, C. S. *Polym. J.* **2009**, *41*, 634–642.
(39) Zabetakis, D.; Dressick, W. J. *ACS Appl. Mater. Interfaces* **2009**, *1*, 4–25.
(40) Lancaster, J. R.; Jehani, J.; Carroll, G. T.; Chen, Y.; Turro, N. J.; Koberstein, J. T. *Chem. Mater.* **2008**, *20*, 6583–6585.
(41) Mévellec, V.; Roussel, S.; Tessier, L.; Chancolon, J.; Mayne-L'Hermite, M.; Deniau, G.; Viel, P.; Palacin, S. *Chem. Mater.* **2007**, *19*, 6323–6330.
(42) Bayramoglu, G.; Metin, A. U.; Arica, M. Y. *Appl. Surf. Sci.* , *256*, 6710–6716.

(43) Wang, X. P.; Chen, Z. F.; Shen, Z. Q. *Sci. China, Ser. B: Chem.* **2005**, *48*, 553–559.
(44) Beamson, G.; Briggs, D. *High Resolution XPS of Organic Polymers: The Scienta ESCA300*; John Wiley & Sons: New York, 1992.
(45) Brandow, S. L.; Dressick, W. J.; Marrian, C. R. K.; Chow, G. M.; Calvert, J. M. *J. Electrochem. Soc.* **1995**, *142*, 2233–2243.
(46) Weast, R. C. *CRC Handbook of Chemistry and Physics*; CRC Press: Boca Raton, 1984.
(47) Aithal, R. K.; Yenamandra, S.; Gunasekaran, R. A.; Coane, P.; Varahramyan, K. *Mater. Chem. Phys.* **2006**, *98*, 95–102.
(48) Schaefers, S.; Rast, L.; Stanishevsky, A. *Mater. Lett.* **2006**, *60*, 706–709.
(49) Brandow, S. L.; Chen, M. S.; Wang, T.; Dulcey, C. S.; Calvert, J. M.; Bohland, J. F.; Calabrese, G. S.; Dressick, W. J. *J. Electrochem. Soc.* **1997**, *144*, 3425–3434.
(50) Jackson, R. L. EU Patent 0 250 867, 1988.

AM100907J